

Chirally motivated $\pi\Sigma - \bar{K}N$ model in a finite volume

Peter C. Bruns^a, Aleš Cieplý^b

¹Nuclear Physics Institute, Czech Academy of Sciences, 250 68 Řež, Czechia

June 30, 2025

Abstract We generalize the chirally motivated $\pi\Sigma - \bar{K}N$ coupled channels model to the cubic finite volume and use it to calculate the stationary energy spectrum that appears in a nice agreement with the spectrum obtained in the lattice QCD simulations by the BaSc collaboration. Several other comparisons with the BaSc results are made, in particular relating their pole positions of the meson-baryon scattering matrix to the two-pole picture of $\Lambda(1405)$ generated by our chiral model in the infinite volume.

Keywords chiral dynamics · meson-baryon interactions · lattice QCD · $\Lambda(1405)$ resonance

PACS 13.75.Jz · 24.10.Eq · 12.38.Gc

1 Introduction

The rigorous study of low-energy strangeness $S = -1$ meson-baryon (MB) scattering is hampered by the fact that neither perturbative QCD nor its low-energy effective field theory, Chiral Perturbation Theory, can be applied without model-dependent non-perturbative extensions in the energy region of interest. Such extensions are necessary due to the presence of an s-wave resonance just below the kaon-nucleon threshold, known as the $\Lambda(1405)$. Notably, almost all modern theoretical approaches which are based on interaction kernels derived from a chiral Lagrangian combined with coupled-channel methods [1–9] come to the conclusion that there are actually *two poles* in the complex-energy plane near the $\bar{K}N$ threshold [10–18].

A rather recent development is the application of lattice QCD (LQCD) to study $\pi\Sigma - \bar{K}N$ scattering

[19, 20], while some work has already been done on the excited states seen in such reactions [21–24]. There, QCD correlators are evaluated on a finite Euclidean space-time lattice employing Monte-Carlo methods to the QCD path integral. To connect the lattice results with the real world, one has to get under control the discretization errors, finite volume (FV) effects, and the extrapolation to physical quark masses. Resonance parameters like mass, width and other properties are not directly accessible from the correlators. Instead, some parametrization for the scattering amplitude is typically used to connect the results for the correlators with the pole position of the resonance on an unphysical Riemann sheet. For narrow isolated resonances, a simple Breit-Wigner parametrization might be sufficient, but for more complicated cases, sophisticated unitary models have to be employed, thereby introducing a model dependence to the analysis. Thus, from the perspective of the coupled-channel models, the lattice results constitute an additional kind of “experimental data” to which the models can be fitted and compared. For the $\Lambda(1405)$, this has been done by several groups in the last few years [25–27]. To assess the inherent model dependence of the various extrapolations, it is desirable to consider a big variety of models, compare their outcome, and eventually find criteria for their quality.

It is the main aim of the present contribution to demonstrate the consistency of the results from a recent LQCD simulation by the Baryon Scattering (BaSc) collaboration [19, 20] with one particular chirally motivated coupled channel model, namely the Prague model developed and studied in [6, 28, 29]. Specifically, we chose its most recent version [29] as a representative example. The generalization of the model to the lattice setting of [20] is quite straightforward, and will be explained only shortly in the next section. The discussion

^ae-mail: bruns@ujf.cas.cz

^be-mail: cieply@ujf.cas.cz

of the results, however, is given in some detail in Sec. 3. In particular, we study the movement of the $\Lambda(1405)$ poles when the volume is sent to infinity, and also (for the infinite volume case) the pole trajectories traversed upon varying the hadron masses and decay constants from their values in the lattice setting to the physical values. All in all, as we state in our summary in Sec. 4, we find a satisfying agreement of the Prague model predictions with the lattice results of [20], and generate some further predictions which can be compared with future lattice simulations.

2 Finite volume model formulation

In the Prague model [29], the s-wave meson-baryon scattering amplitude is of the form

$$f_{0+}(s) = g(s)[1 - v_{0+}(s)G(s)]^{-1}v_{0+}(s)g(s). \quad (1)$$

Here v_{0+} is the s-wave projection of the interaction kernel as derived for the chiral MB Lagrangian, G is a loop function describing the propagation of a MB pair, and the Yamaguchi form factors $g(q) = 1/[1 + (q/\alpha)^2]$ provide the means to regularize the loop function integral with the parameters α representing regularization scales. In Eq. (1) we use the notation $g(s) \equiv g(q(s))$, where $q(s)$ is the modulus of the center-of-mass (c.m.) momentum for the meson-baryon system for c.m. energy \sqrt{s} , see Eq. (10) in Appendix B. The building blocks of f_{0+} are coupled-channel matrices, and its form is dictated by the strategy of re-summation of loop graphs with arbitrarily many insertions of the separable interaction kernel v_{0+} . This construction principle remains unchanged when restricting the model to a finite cubic lattice volume. Most importantly, the interaction kernel also remains unchanged, since it does not contain contributions from long-range exchanges (like e.g. pion-exchange graphs), and we neglect exponentially suppressed FV corrections to masses and coupling constants. Strictly speaking, we should also modify the partial-wave projection, since rotational symmetry is broken on a cubic lattice. However, since the Prague model so far has a reliable parametrization only of the s-wave amplitude, such an attempt would be futile at this point. Thus, we have to restrict ourselves to the analysis of lattice states pertaining to irreducible representations of the cubic group which have a dominant overlap with infinite volume s-wave states.

The general framework of quantum theories in a finite volume is well known [30–34]. Here, we follow the same strategy as e.g. [25, 26, 35, 36] and modify only the loop function G in our scattering amplitude Eq. (1).

In the infinite volume, the MB loop function employed in the Prague model [29] is defined as

$$G_{\text{P}}(q) = 4\pi \int \frac{d^3l}{(2\pi)^3} \frac{[g(l)]^2}{l^2 - q^2 - i\epsilon} = [g(q)]^2 \left(\frac{\alpha^2 - q^2}{2\alpha} + i q \right), \quad (2)$$

where $l^2 \equiv |\vec{l}|^2$. Despite its simple non-relativistic appearance, our loop function has the correct relativistic absorptive part $\sim iq$ due to the use of relativistic kinematics, see Eq. (10) in Appendix B. The form factors $g(l)$ regulate the propagation of particles with momenta $l \lesssim \alpha$ and have provided a convenient tool for extrapolations of the MB amplitudes off-the-energy shell since their introduction when the adopted coupled-channel model was designed in [1]. A comparison with an alternative of dimensionally regularized loop function was given e.g. in [37], see the discussion following Eq. (2.11) there.

We need to generalize Eq. (2) to the case of a cubic FV $V = L^3$. For a free particle inside a finite cube of side length L , with periodic boundary conditions, the possible three-momenta are $\vec{p}_n = \frac{2\pi}{L}\vec{n}$, $\vec{n} \in \mathbb{Z}^3$. The discretization of the integral in Eq. (2) is straightforward and yields

$$G_{\text{P}}^{\text{FV}}(q; L) = \frac{4\pi}{L^3} \sum_{\vec{n} \in \mathbb{Z}^3} \frac{[g(p_n)]^2}{p_n^2 - q^2}. \quad (3)$$

Note that the summands depend only on $n^2 := |\vec{n}|^2$, and therefore we can just sum over this variable, with a weight factor $w(n^2)$ counting the multiplicity of lattice points \vec{n} with a given n^2 , $w(n^2) = 1, 6, 12, 8, 6, \dots$ for $n^2 = 0, 1, 2, 3, 4, \dots$. Some additional details related to computation of the MB loop function are given in Appendix A.

Obviously, the formula Eq. (3) can be used as it is when analyzing the properties of the MB coupled channel system in the finite cubic volume. However, it should be noted that the series of poles present at the discrete momenta $q = \pm p_n$ replaces a branch cut inherent in the infinite volume loop function Eq. (2) due to the multi-valued character of the momentum q as a function of the Mandelstam variable s . Thus, there is no natural analogue of a second-sheet FV loop function via analytic continuation. However, one can devise expressions that approach the infinite volume physical sheet and second sheet loop functions for $L \rightarrow \infty$ everywhere except on the branch cut, see Appendix B.

When evaluating the FV loop function at complex energies (and momenta) away from the real axis we found it most convenient to use the generalized formulas

$$G_{\text{P}}^{\text{FV}}(q; L) = [g(q)]^2 \left[\tilde{G}_{\text{P}}(q) + \Delta \tilde{G}_{\mathcal{R}}(q; L) + \Delta \tilde{G}_{\mathcal{I}}(q; L) \right],$$

$$\Delta\tilde{G}_{\mathcal{R}}(q; L) = \sum_{\vec{0} \neq \vec{n} \in \mathbb{Z}^3} e^{-n\alpha L}, \quad (4)$$

$$\Delta\tilde{G}_{\mathcal{I}}(q; L) = \sum_{\vec{0} \neq \vec{n} \in \mathbb{Z}^3} \frac{1}{nL} [e^{\pm iqnL} - (1 + n\alpha L)e^{-n\alpha L}],$$

where $n = |\vec{n}|$, the \pm sign in the exponent on the last line matches the sign of the imaginary part of the momentum q , and the tilded G -functions stand for the loop function parts divided by the form-factor $g(q)$ squared, e.g. $G_P(q) = [g(q)]^2 \tilde{G}_P(q)$. The terms $\Delta\tilde{G}_{\mathcal{R}}(q; L)$ and $\Delta\tilde{G}_{\mathcal{I}}(q; L)$ represent FV corrections to the first (*pseudo-real*) and second (*phase-space*) parts of the infinite volume loop function, Eq. (2), and apparently vanish in the $L \rightarrow \infty$ limit. We also note that, for a fixed L -value, the oscillations caused by the $\exp(\pm iqnL)$ term in $\Delta\tilde{G}_{\mathcal{I}}(q; L)$ are better suppressed at complex energies further from the real axis.

3 Results and discussion

We start our analysis by looking at the hadron masses used by the BaSc collaboration, see Table III in their paper [20]. While the kaon mass there, $M_K \approx 486$ MeV, is relatively close to the physical value, their pion mass $M_\pi \approx 204$ MeV still remains somewhat off, a common feature of present-day lattice simulations. However, we find it interesting that all BaSc hadron masses are very close to the trajectories of hadron masses adopted in [29] when going to the SU(3) flavor symmetric limit, see the Appendix there. We demonstrate it in Fig. 1, where the masses follow the paths from the SU(3) flavor symmetric point (for the scaling factor $x_{\text{SU}3} = 0$) to their physical values (at $x_{\text{SU}3} = 1$). As one can see, the BaSc hadron masses are very close to the depicted trajectories for $x_{\text{SU}3} \approx 0.86$. The latter value can be viewed as an indication of how far are the LQCD predictions from the physical reality.

Let us follow this observation by a presentation and discussion of some results obtained with the chirally motivated $\pi\Sigma - \bar{K}N$ coupled channel model of Ref. [29] (also referred to as the P0 model in the following text) re-formulated in the finite volume. If not specified otherwise, all our FV calculations were performed with $L = 20$ GeV $^{-1}$, a value approximately matching the spatial extent $L = 4.051$ fm used in [20]. In Fig. 2 we present the calculated elastic isoscalar $\bar{K}N$ amplitudes, plotted as a function of the c.m. energy, for both the FV and infinite-volume formulations of the P0 model. Since the FV loop-function, Eq. (3), is manifestly real for real c.m. energies, so is the pertinent $\bar{K}N$ amplitude visualized by the red dotted lines. The real (continuous blue) and imaginary (dashed blue) parts of the amplitudes in the infinite volume are shown for comparison

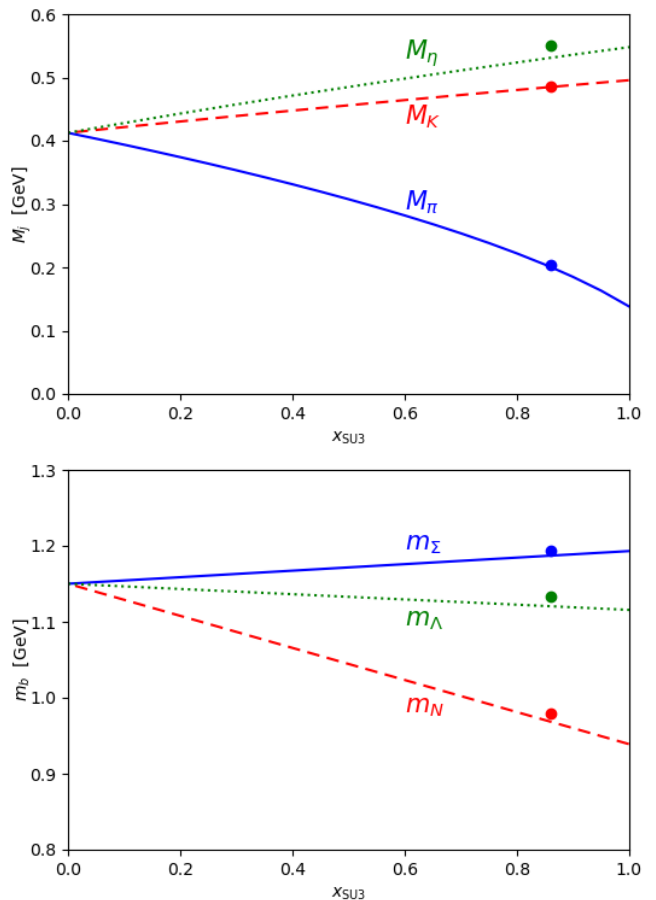


Fig. 1 The parametrization of hadron masses used in [29] as a function of the $x_{\text{SU}3}$ parameter that measures the amount of SU(3) flavor-symmetry breaking. The BaSc masses shown at $x_{\text{SU}3} = 0.86$ are marked with the full dots. Top panel - meson masses, bottom panel - baryon masses.

in the same Figure. In the top panel, the physical values of hadron masses and meson decay constants were used in the calculation, so the infinite volume curves correspond to those for the K^-p amplitude presented in Fig. 2 in [29]. In the bottom panel, the BaSc masses and meson decay constants were used and the channel thresholds are shifted accordingly. The unphysical hadron masses in this panel also lead to unphysical $\bar{K}N$ amplitudes including the one generated for the infinite volume. Though, it is worth noting the sharp variation of this amplitude around the (shifted) $\pi\Sigma$ threshold implying a nearby pole of the amplitude at the real axis or in its vicinity, a point we will discuss later on.

The FV amplitudes exhibit divergencies that relate to the poles realized at the points where $q^2 = p_n^2 = (2\pi/L)^2 n^2$ when the MB loop function Eq. (3) is used instead of Eq. (2) to generate the s-wave scattering amplitudes f_{0+} . We have kept in Fig. 2 the red dotted vertical lines that cross the real axis at points, where the

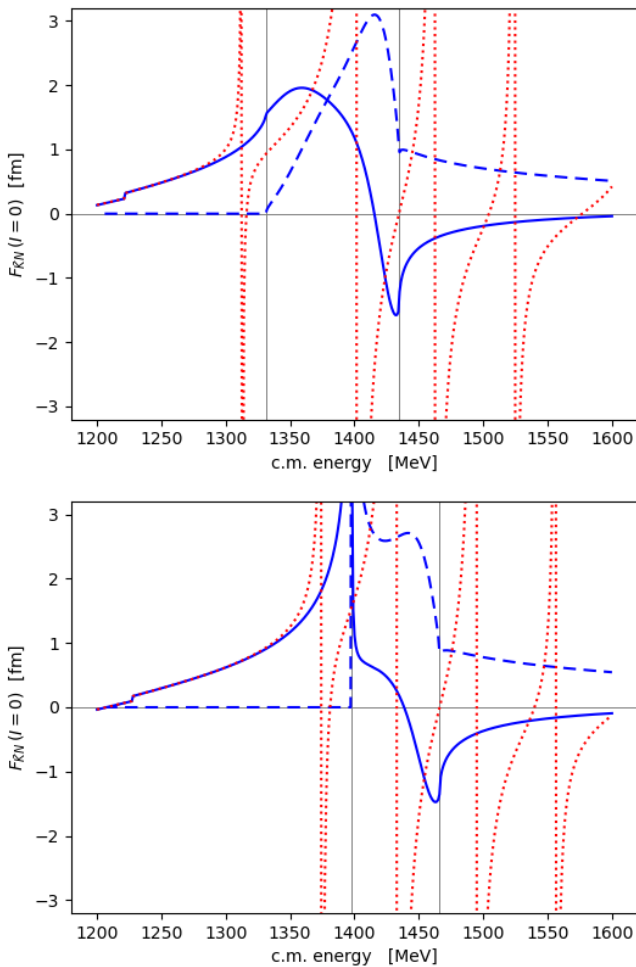


Fig. 2 The elastic isoscalar $\bar{K}N$ amplitude calculated in the finite volume for $L = 20 \text{ GeV}^{-1}$ (dotted red lines) is compared with the real (continuous blue) and imaginary (dashed blue) parts of the amplitude generated by the Prague P0 model [29]. The gray vertical lines mark the positions of the $\pi\Sigma$ and $\bar{K}N$ thresholds. Top panel - results for the physical hadron masses and meson decay constants, bottom panel - the same for the BaSc masses and decay constants.

amplitude values switch from $+\infty$ to $-\infty$. These points define the FV stationary energies that correspond to those reported in the LQCD calculations. In [20], the BaSc collaboration used the energy spectra of several irreducible lattice representations in fits of selected K -matrix coupled-channel models following a procedure outlined in [38] and utilized to make a connection to the real physical world. While their approach was fine to establish the existence of two poles of the scattering amplitude in the $\Lambda(1405)$ region, it was restricted to only two channels (the $\pi\Sigma$ and $\bar{K}N$ ones) and the adopted K -matrix models themselves are not as sophisticated as the modern coupled channels approaches based on interactions derived from the chiral Lagrangian.

In principle, we could also tune the Prague model parameters to fit the BaSc energy spectra generated for the irreps shown in [20] but it would be a more involved task. In the present work we just demonstrate how our finite-volume model does in comparison with the BaSc energy spectrum of the $G_{1u}(0)$ irrep that seems most relevant when one considers only the s-wave. In Table 1 we present the stationary state energies generated by our FV model for two parameter settings, P0 and P2 taken from [29, 39], and the BaSc energy spectrum of the $G_{1u}(0)$ irrep extracted from Fig. 8 in [20]. The P0 spectrum matches exactly the energies of divergencies observed in the bottom panel of Fig. 2 and the energy variations shown for the P0 and P2 spectra were obtained by varying the spatial extent by $\Delta L = 1 \text{ GeV}^{-1}$, a value about 3 times larger than the standard deviation of the L -value adopted in [20]. The two lowest energies (both below the $\bar{K}N$ threshold) appear particularly stable with respect to the L -variations in our model. It should be noted that the P2 model does not reproduce the K^-p reactions data so well as the P0 model does due to complementing the model fit with the $\pi\Sigma$ photoproduction data. The P2 parameter setting is also closely related to a specific construction of the photoproduction kernel, see [39] for details, and does not provide realistic predictions at higher energies, e.g. for the $\Lambda(1670)$ pole position. Therefore, the P0 model results should be regarded more seriously while the P2 model spectrum of FV stationary energies was included in Table 1 just to demonstrate a possible model dependence. As one can see, the correspondence between the P0 and BaSc energy spectra is remarkably good with only one energy being off by more than one standard deviation reported for the $G_{1u}(0)$ irrep. We would like to emphasize the point that these two energy spectra result from two very different approaches to QCD, one being the $\pi\Sigma - \bar{K}N$ coupled channel model based on chiral dynamics with parameters fitted to real physics data and the other the LQCD simulations of the MB interactions. It is really encouraging to see that so nice mutual agreement can be reached between these two distinctly different worlds.

P0 energies [MeV]	P2 energies [MeV]	BaSc energies [MeV]
1375 ± 2	1371 ± 2	1374 ± 8
1432 ± 1	1429 ± 1	1447 ± 9
1494 ± 6	1509 ± 8	1495 ± 13
1556 ± 12	1594 ± 16	1566 ± 12

Table 1 A comparison of the finite volume stationary state energies generated by the P0 and P2 models from [39] with those obtained by the BaSc collaboration [20] for the $G_{1u}(0)$ irreducible representation.

We now turn our attention to the poles of the scattering matrix. The Eq. (4) enables us to search for the poles of the FV amplitudes in the whole complex energy manifold. When performing the calculation with physical hadron masses and meson decay constants, for sufficiently large space volume (in the limit $L \rightarrow \infty$), we should be able to recover the pole positions generated in the original P0 model. We demonstrate this in Table 2, where the pole positions are specified for increasing values of L . Since the typical values of the regularization scales are $\alpha \approx 0.3 - 0.7$ GeV, the finite volume correction $\Delta\tilde{G}_{\mathcal{R}}(q; L) \sim e^{-\alpha L}$ is quite small already for the lowest considered value $L = 20$ GeV $^{-1}$. The other FV correction $\Delta\tilde{G}_{\mathcal{I}}(q; L)$ is more significant as its leading term in L is proportional to $\exp(\pm iqL)/L$ and it takes larger L -values to suppress it. As we also mentioned in Sec. 2, the Eq. (4) works better for complex energies further from the real axis which is reflected by the convergence of the two $\Lambda(1405)$ poles to their infinite volume positions. We have found that the z_1 pole reaches the latter for $L \approx 90$ (with the precision of 0.1 MeV used in the Table) while $L \approx 190$ is needed for the z_2 pole.

L [1/GeV]	z_1 [MeV]	z_2 [MeV]
20	(1365.8, -72.2)	(1569.8, -30.9)
40	(1350.7, -46.4)	(1425.0, -24.5)
60	(1352.0, -42.4)	(1426.2, -21.1)
80	(1352.8, -42.6)	(1429.1, -26.1)
100	(1352.7, -42.8)	(1429.5, -22.7)
∞	(1352.7, -42.8)	(1428.5, -23.7)

Table 2 The convergence of the generated pole positions to their infinite volume ones [29] is demonstrated for increasing values of the lattice spatial extent L .

Next, we would like to demonstrate how the pole positions found by the BaSc collaboration are related to those generated by the chirally motivated $\pi\Sigma - \bar{K}N$ coupled channel approaches. Once again, we make use of the P0 Prague model as a representative example of the latter and follow the movement of the poles when one varies the hadron masses and meson decay constants from their physical values to those adopted by the BaSc collaboration (and vice versa). In Fig. 3 we show the pole movements while the physical quantities are varied according to

$$\mathcal{Y}(x) = \mathcal{Y}_{\text{BaSc}} + x(\mathcal{Y}_{\text{phys}} - \mathcal{Y}_{\text{BaSc}}), \quad (5)$$

where \mathcal{Y} represents the involved hadron masses and decay constants, and the linear scaling factor $x \in \langle 0, 1 \rangle$. The positions of the $\pi\Sigma$ and $\bar{K}N$ thresholds in the physical ($x = 1$) and BaSc ($x = 0$) limits are visualized in the Figure by the continuous and dotted vertical

lines, respectively. While the top panel shows the movement of the poles when all hadron masses and meson decay constants are varied, the bottom panel demonstrates the impact of varying only the pion mass. Obviously, the $\bar{K}N$ threshold does not move in the latter case and the pertinent dotted and continuous lines coincide in the bottom panel.

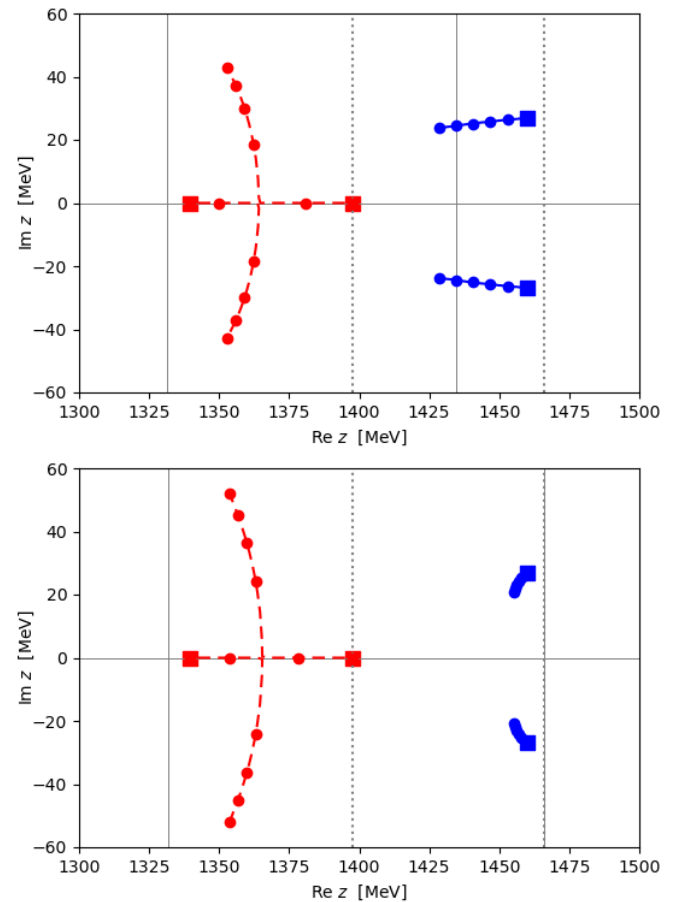


Fig. 3 The pole trajectories upon varying the hadron masses and meson decay constants from their lattice QCD values to those in the physical limit. The full squares show the pole positions for the former while the dots mark pole positions for the increasing scaling factor x in steps of 0.2, the last point at $x = 1$. Top panel - all hadron masses and meson decay constants are varied, bottom panel - only the pion mass is varied while all the other masses and decay constants are kept fixed at their lattice QCD values.

The pole trajectories presented in the top panel of Fig. 3 clearly demonstrate that the pole positions found by the BaSc collaboration are related to those generated by the P0 model and it is natural to extrapolate that the same conclusion can be reached with the other chirally motivated coupled channel approaches. In particular, the virtual state reported close to the $\pi\Sigma$ threshold in [19, 20] transforms into the lower mass $\Lambda(1405)$

pole when the hadron masses get to their physical values. We have checked that the variations of the meson decay constants have a negligible impact in this respect, most likely because their LQCD values used by the BaSc collaboration are already quite close to the physical ones. In fact, only the LQCD values of the pion and nucleon masses are significantly off their physical counterparts, which we have seen in Fig. 1 as well. The bottom panel of Fig. 3 shows that the non-physical pion mass used in the LQCD simulations is likely the main reason why a virtual state was found instead of a resonance in [19, 20], see also [18]. Indeed, as the pion mass is gradually restored to its physical value, the pole transforms into a proper resonant one. It is also worth noting that besides the pole close to the $\pi\Sigma$ threshold (the FV extension of the P0 model has it on the physical Riemann sheet, just marginally below the threshold) there is another pole further below the threshold at the $x = 0$ limit. Its existence was not reported by the BaSc collaboration, but it is required by the analytical properties of the $\pi\Sigma - \bar{K}N$ coupled channel model. When one follows the movement of the two conjugate poles from their $x = 1$ positions in Fig. 3, they meet at the real axis (for $x \approx 0.28$ in the top panel) and then move along the real axis in opposite directions. Thus, there must be two poles in the $x = 0$ limit.

It is also well known that a presence of resonant states in FV simulations can be identified when one analyses the L -dependence of the stationary state energies [31]. In Fig. 4 we follow this idea utilizing the P0 model from [29] and show the L -dependence of ten lowest energies. The top panel presents the results obtained with the physical hadron masses and meson decay constants while in the bottom panel the BaSc values were used for these quantities. The four lowest stationary energies at $L = 20 \text{ GeV}^{-1}$ match the positions of discontinuities observed for the FV $\bar{K}N$ amplitude in the respective top and bottom panels of Fig. 2. According to [31], an appearance of the energy plateaus and the pertinent avoided energy levels crossings, that can be clearly noted in Fig. 4, is directly related to an existence of a resonance in the studied system. In the top panel, the plateau emerges at $E \approx 1435 \text{ MeV}$, an energy only about 7 MeV larger when compared with the infinite volume position of the (higher in mass) z_2 pole shown in Table 2. The difference can be attributed to the coupled channels effects, in particular to the existence of the second $\Lambda(1405)$ pole generated by the chiral dynamics. On the other hand, the energy plateau at $E \approx 1460 \text{ MeV}$ observed in the bottom panel of Fig. 4 almost exactly matches the position of the pole at $z = (1460, -27) \text{ MeV}$ that our model generates for

the BaSc setting in which the second pole degenerates into a state no longer recognized as another resonance.

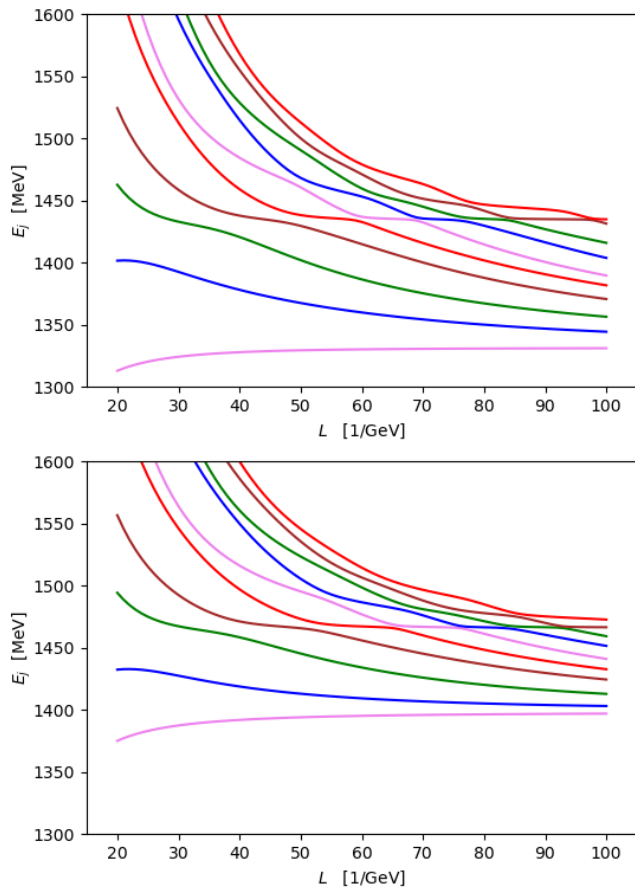


Fig. 4 The L -dependence of the finite volume energy spectra. Top panel - physical hadron masses and meson decay constants used to generate the ten lowest stationary state energies (Prague P0 model [29]), bottom panel - BaSc hadron masses and meson decay constants used.

4 Summary

We have presented a simple generalization of the chirally motivated $\pi\Sigma - \bar{K}N$ Prague model [29] to the cubic finite volume. The FV formulation of the MB loop function enabled us to calculate the stationary energy levels of the coupled channel system and compare them with the appropriate $G_{1u}(0)$ irrep spectrum obtained recently by the BaSc collaboration [19, 20]. Both spectra were found in remarkably good agreement, which provides a confidence for making more comparisons of our FV model with the LQCD simulations. We also find it interesting (and in a way encouraging) that the hadron masses used by the BaSc collaboration are quite close to the mass trajectories adopted in [29] when go-

ing to the $SU(3)$ flavor symmetric point. The credibility of our FV model was also checked by confirming that the two poles of the scattering matrix found on the complex energy plane in the FV regime converge to the pole positions reported in [29] when the cubic volume goes to infinity, i.e. the spatial extent $L \rightarrow \infty$.

We have demonstrated that two poles of the scattering matrix found in the complex energy plane by the BaSc collaboration, a resonance just below the $\bar{K}N$ threshold and another one on the real axis close to the $\pi\Sigma$ threshold, transform into the standard two pole picture of $\Lambda(1405)$ when one reconciles gradually the LQCD hadron masses (and meson decay constants) with their physical values. We have also shown that the relatively large pion mass used in the LQCD simulations represents the main reason why one of the resonance poles (the one at lower mass and further from the real axis) degenerated into a virtual state reported by the BaSc collaboration.

Finally, we have also looked at the L -dependence of the stationary energy spectra and shown that they exhibit features compatible with the discussed pole structure of the scattering matrix for both our FV version of the $\pi\Sigma - \bar{K}N$ Prague model as well as for the BaSc setting.

Acknowledgments

We would like to thank B. Cid-Mora for a helpful communication concerning the stationary energy spectra generated by the BaSc collaboration.

Appendix A Loop function in a finite volume

When deriving the FV loop function $G_{\mathbb{P}}^{\text{FV}}$ we found it convenient to separate it into a regularization-dependent *pseudo-real part* and a *phase-space part*. To this end, let us consider an integral representation for the phase-space part in the infinite volume,

$$i q = 4\pi \int \frac{d^3 l}{(2\pi)^3} \left[\frac{1}{l^2 - q^2 - i\epsilon} - \frac{l^2 + 3\alpha^2}{(l^2 + \alpha^2)^2} \right]. \quad (6)$$

Going to a finite volume, we replace the integral on the r.h.s. by a sum, multiply it with $[g(q)]^2$, and subtract the outcome from our result for $G_{\mathbb{P}}^{\text{FV}}$ in Eq. (3):

$$G_{\mathcal{R}}^{\text{FV}}(q; L) := G_{\mathbb{P}}^{\text{FV}}(q; L) - [g(q)]^2 \frac{4\pi}{L^3} \sum_{\vec{n} \in \mathbb{Z}^3} \left[\frac{1}{p_n^2 - q^2} - \frac{p_n^2 + 3\alpha^2}{(p_n^2 + \alpha^2)^2} \right] = [g(q)]^2 \frac{4\pi}{L^3} \sum_{\vec{n} \in \mathbb{Z}^3} \frac{\alpha^2 - q^2}{(p_n^2 + \alpha^2)^2}, \quad (7)$$

where the eligible discrete MB momenta are $\vec{p}_n = \frac{2\pi}{L}\vec{n}$. The poles in q^2 have dropped out in Eq. (7), and the sum converges for all real q^2 . The FV corrections in $G_{\mathcal{R}}^{\text{FV}}$ are exponentially suppressed, as one can easily show employing the Poisson summation formula (PSF):

$$\begin{aligned} \tilde{G}_{\mathcal{R}}^{\text{FV}}(q; L) &= G_{\mathcal{R}}^{\text{FV}}(q; L)/[g(q)]^2 = 4\pi(\alpha^2 - q^2) \int \frac{d^3 l}{(2\pi)^3} \left(\frac{2\pi}{L} \right)^3 \sum_{\vec{n} \in \mathbb{Z}^3} \frac{\delta^3(\vec{l} - \vec{p}_n)}{(l^2 + \alpha^2)^2} \\ &\stackrel{\text{PSF}}{=} 4\pi(\alpha^2 - q^2) \int \frac{d^3 l}{(2\pi)^3} \sum_{\vec{k} \in \mathbb{Z}^3} \frac{e^{iL(\vec{k}\cdot\vec{l})}}{(l^2 + \alpha^2)^2} = \frac{\alpha^2 - q^2}{2\alpha} \sum_{\vec{k} \in \mathbb{Z}^3} e^{-\alpha L|\vec{k}|} \\ &= \frac{\alpha^2 - q^2}{2\alpha} \left(1 + 6e^{-\alpha L} + 12e^{-\sqrt{2}\alpha L} + 8e^{-\sqrt{3}\alpha L} + \dots \right). \end{aligned} \quad (8)$$

The first few terms of the expansion given in the last line yield a good approximation for $\alpha L \gtrsim 4$. Note that for real q the first term in the expansion is equal to the real part of the infinite-volume loop function of Eq. (2).

Formally, one can apply similar manipulations to the phase space (*pseudo-imaginary*) part:

$$\begin{aligned} \tilde{G}_{\mathcal{I}}^{\text{FV}}(q; L) &= G_{\mathcal{I}}^{\text{FV}}(q; L)/[g(q)]^2 = 4\pi \int \frac{d^3 l}{(2\pi)^3} \left(\frac{2\pi}{L} \right)^3 \sum_{\vec{n} \in \mathbb{Z}^3} \delta^3(\vec{l} - \vec{p}_n) \left[\frac{1}{l^2 - q^2} - \frac{l^2 + 3\alpha^2}{(l^2 + \alpha^2)^2} \right] \\ &\stackrel{\text{PSF}}{=} \dots \\ &= \pm i q + \sum_{\vec{0} \neq \vec{k} \in \mathbb{Z}^3} \frac{1}{|\vec{k}|L} \left(e^{\pm i q L |\vec{k}|} - (1 + \alpha L |\vec{k}|) e^{-\alpha L |\vec{k}|} \right), \end{aligned} \quad (9)$$

where the plus and minus signs in \pm correspond to $\text{Im } q > 0$ and $\text{Im } q < 0$, respectively. This expansion is not useful for real q , because it diverges at $q = \pm p_n$, and the oscillations of the $\exp(\pm i q L |\vec{k}|)$ terms are not damped. However, for complex q away from the real axis, the first few terms yield a decent approximation for sufficiently large L . Note that there is some (exponentially suppressed) dependence on the real range parameter α , which originates from the second term in Eq. (6) and drops out in the infinite volume.

Appendix B Second Riemann sheet treatment

The loop function in the infinite volume, Eq. (2), is usually considered as a function of the Mandelstam variable s (the squared c.m. energy), setting

$$q \rightarrow q(s) := \frac{1}{2\sqrt{s}} \sqrt{[s - (m_b + M_j)^2][s - (m_b - M_j)^2]}, \quad (10)$$

where m_b and M_j denote the baryon and meson masses, respectively. The square root should be defined in a way that it is positive for real $s > (m_b + M_j)^2$, and has a branch cut on the interval $((m_b + M_j)^2, \infty)$. We conventionally denote by q the branch of the function that has a non-negative imaginary part. The branch cut

structure is inherited by $G_P(s)$, whose analytic continuation on the *second sheet*, traversing the branch cut from above, is then given by

$$G_P^{\text{II}}(s) = \frac{[\alpha - iq(s)]^2}{2\alpha} [g(q(s))]^2, \quad (11)$$

i.e. the sign of the iq term is reversed. Since in the FV expression Eq. (3) the branch cut is replaced by a series of poles, there is no natural analogue of a second-sheet function via analytic continuation. Fortunately, one can utilize the Eqs. (8 - 9) and postulate

$$G_P^{\text{FV(I)}}(s; L) = G_{\mathcal{R}}^{\text{FV}}(s; L) + G_{\mathcal{I}}^{\text{FV}}(s; L), \quad (12)$$

$$G_P^{\text{FV(II)}}(s; L) = G_{\mathcal{R}}^{\text{FV}}(s; L) - G_{\mathcal{I}}^{\text{FV}}(q; L), \quad (13)$$

with the plus sign (due to the chosen q branch) taken in $G_{\mathcal{I}}^{\text{FV}}$. As one can easily check, these expressions approach the infinite volume physical sheet and second sheet loop functions for $L \rightarrow \infty$ everywhere except on the branch cut. Alternatively, one could also define q such that $\text{Im} q < 0$ in the lower complex s -plane, and use the $G_{\mathcal{I}}^{\text{FV}}$ of Eq. (9) with a negative sign in Eq. (13).

References

1. N. Kaiser, P. B. Siegel, and W. Weise, “Chiral dynamics and the low-energy kaon-nucleon interaction,” *Nucl. Phys. A*, vol. 594, pp. 325–345, 1995.
2. E. Oset and A. Ramos, “Nonperturbative chiral approach to s wave $\bar{K}N$ interactions,” *Nucl. Phys. A*, vol. 635, pp. 99–120, 1998.
3. B. Krippa, “Chiral dynamics of the low-energy kaon-baryon interactions,” *Phys. Rev. C*, vol. 58, pp. 1333–1336, 1998.
4. C. Garcia-Recio, J. Nieves, E. Ruiz Arriola, and M. J. Vicente Vacas, “ $S = -1$ meson baryon unitarized coupled channel chiral perturbation theory and the $S(01)$ $\Lambda(1405)$ and $\Lambda(1670)$ resonances,” *Phys. Rev. D*, vol. 67, p. 076009, 2003.
5. B. Borasoy, R. Nißler, and W. Weise, “Chiral dynamics of kaon-nucleon interactions, revisited,” *Eur. Phys. J. A*, vol. 25, pp. 79–96, 2005.
6. A. Cieplý and J. Smejkal, “Chirally motivated $\bar{K}N$ amplitudes for in-medium applications,” *Nucl. Phys. A*, vol. 881, pp. 115–126, 2012.
7. Y. Ikeda, T. Hyodo, and W. Weise, “Chiral SU(3) theory of antikaon-nucleon interactions with improved threshold constraints,” *Nucl. Phys. A*, vol. 881, pp. 98–114, 2012.
8. Z.-H. Guo and J. A. Oller, “Meson-baryon reactions with strangeness -1 within a chiral framework,” *Phys. Rev. C*, vol. 87, no. 3, p. 035202, 2013.
9. A. Feijoo, V. Magas, and A. Ramos, “ $S = -1$ meson-baryon interaction and the role of isospin filtering processes,” *Phys. Rev. C*, vol. 99, no. 3, p. 035211, 2019.
10. J. A. Oller and U.-G. Meißner, “Chiral dynamics in the presence of bound states: Kaon nucleon interactions revisited,” *Phys. Lett. B*, vol. 500, pp. 263–272, 2001.
11. D. Jido, J. A. Oller, E. Oset, A. Ramos, and U.-G. Meißner, “Chiral dynamics of the two $\Lambda(1405)$ states,” *Nucl. Phys. A*, vol. 725, pp. 181–200, 2003.
12. T. Hyodo and D. Jido, “The nature of the $\Lambda(1405)$ resonance in chiral dynamics,” *Prog. Part. Nucl. Phys.*, vol. 67, pp. 55–98, 2012.
13. M. Mai and U.-G. Meißner, “New insights into antikaon-nucleon scattering and the structure of the $\Lambda(1405)$,” *Nucl. Phys. A*, vol. 900, pp. 51 – 64, 2013.
14. A. Cieplý, M. Mai, U.-G. Meißner, and J. Smejkal, “On the pole content of coupled channels chiral approaches used for the $\bar{K}N$ system,” *Nucl. Phys. A*, vol. 954, pp. 17–40, 2016.
15. P. C. Bruns and A. Cieplý, “Importance of chiral constraints for the pole content of the $\bar{K}N$ scattering amplitude,” *Nucl. Phys. A*, vol. 996, p. 121702, 2020.
16. U.-G. Meißner, “Two-pole structures in QCD: Facts, not fantasy!,” *Symmetry*, vol. 12, no. 6, p. 981, 2020.
17. M. Mai, “Review of the $\Lambda(1405)$ A curious case of a strangeness resonance,” *Eur. Phys. J. ST*, vol. 230, no. 6, pp. 1593–1607, 2021.

18. J.-M. Xie, J.-X. Lu, L.-S. Geng, and B.-S. Zou, “Two-pole structures as a universal phenomenon dictated by coupled-channel chiral dynamics,” *Phys. Rev. D*, vol. 108, no. 11, p. L111502, 2023.
19. J. Bulava *et al.*, “Two-pole nature of the $\Lambda(1405)$ resonance from lattice QCD,” *Phys. Rev. Lett.*, vol. 132, no. 5, p. 051901, 2024.
20. J. Bulava *et al.*, “Lattice QCD study of $\pi\Sigma - \bar{K}N$ scattering and the $\Lambda(1405)$ resonance,” *Phys. Rev. D*, vol. 109, no. 1, p. 014511, 2024.
21. T. T. Takahashi and M. Oka, “Low-lying lambda baryons with spin 1/2 in two-flavor lattice QCD,” *Phys. Rev. D*, vol. 81, p. 034505, 2010.
22. T. Burch, C. Gatttringer, L. Y. Glozman, C. Hagen, D. Hierl, C. B. Lang, and A. Schäfer, “Excited hadrons on the lattice: Baryons,” *Phys. Rev. D*, vol. 74, p. 014504, 2006.
23. G. P. Engel, C. B. Lang, and A. Schäfer, “Low-lying Λ baryons from the lattice,” *Phys. Rev. D*, vol. 87, no. 3, p. 034502, 2013.
24. J. M. M. Hall, W. Kamleh, D. B. Leinweber, B. J. Menadue, B. J. Owen, A. W. Thomas, and R. D. Young, “Lattice QCD Evidence that the $\Lambda(1405)$ Resonance is an Antikaon-Nucleon Molecule,” *Phys. Rev. Lett.*, vol. 114, no. 13, p. 132002, 2015.
25. A. Martinez Torres, M. Bayar, D. Jido, and E. Oset, “Strategy to find the two $\Lambda(1405)$ states from lattice QCD simulations,” *Phys. Rev. C*, vol. 86, p. 055201, 2012.
26. R. Molina and M. Döring, “Pole structure of the $\Lambda(1405)$ in a recent QCD simulation,” *Phys. Rev. D*, vol. 94, no. 5, p. 056010, 2016. [Addendum: *Phys.Rev.D* 94, 079901 (2016)].
27. R. Pavao, P. Gubler, P. Fernandez-Soler, J. Nieves, M. Oka, and T. T. Takahashi, “The negative-parity spin-1/2 Λ baryon spectrum from lattice QCD and effective theory,” *Phys. Lett. B*, vol. 820, p. 136473, 2021.
28. A. Cieplý and J. Smejkal, “Separable potential model for K^-N interactions at low energies,” *Eur. Phys. J. A*, vol. 43, pp. 191–208, 2010.
29. P. C. Bruns and A. Cieplý, “SU(3) flavor symmetry considerations for the $\bar{K}N$ coupled channels system,” *Nucl. Phys. A*, vol. 1019, p. 122378, 2022.
30. M. Lüscher, “Volume Dependence of the Energy Spectrum in Massive Quantum Field Theories. 1. Stable Particle States,” *Commun. Math. Phys.*, vol. 104, p. 177, 1986.
31. U. J. Wiese, “Identification of Resonance Parameters From the Finite Volume Energy Spectrum,” *Nucl. Phys. B Proc. Suppl.*, vol. 9, pp. 609–613, 1989.
32. P. Hasenfratz and H. Leutwyler, “Goldstone Boson Related Finite Size Effects in Field Theory and Critical Phenomena With $O(N)$ Symmetry,” *Nucl. Phys. B*, vol. 343, pp. 241–284, 1990.
33. M. Lüscher, “Two particle states on a torus and their relation to the scattering matrix,” *Nucl. Phys. B*, vol. 354, pp. 531–578, 1991.
34. M. Lüscher, “Signatures of unstable particles in finite volume,” *Nucl. Phys. B*, vol. 364, pp. 237–251, 1991.
35. M. Döring, U.-G. Meißner, E. Oset, and A. Rusetsky, “Unitarized Chiral Perturbation Theory in a finite volume: Scalar meson sector,” *Eur. Phys. J. A*, vol. 47, p. 139, 2011.
36. D. Severt and U.-G. Meißner, “The Roper Resonance in a finite volume,” *Commun. Theor. Phys.*, vol. 72, no. 7, p. 075201, 2020.
37. P. C. Bruns, A. Cieplý, and M. Mai, “Testing chiral unitary models for the $\Lambda(1405)$ in $K^+\pi\Sigma$ photoproduction,” *Phys. Rev. D*, vol. 106, no. 7, p. 074017, 2022.
38. C. Morningstar, J. Bulava, B. Singha, R. Brett, J. Fallica, A. Hanlon, and B. Hörz, “Estimating the two-particle K -matrix for multiple partial waves and decay channels from finite-volume energies,” *Nucl. Phys. B*, vol. 924, pp. 477–507, 2017.
39. A. Cieplý and P. C. Bruns, “Constraining the chirally motivated $\pi\Sigma - \bar{K}N$ models with the $\pi\Sigma$ photoproduction mass spectra,” *Nucl. Phys. A*, vol. 1043, p. 122819, 2024.